Current Science
CS 5 (3), 2468-2478 (2025)
Received 21 Feb 2025 | **Revised** 18 March 2025 | **Accepted** 20 April. 2025 | **Online Available** 19 May 2025
https://doi.org/ 10.52845/CS/2025-5-3-33

Current Science

Current Science

OPEN ACCESS

ISSN(O)2795-8639

Original Article

The Application of Improved Small Sub-Domain Filtering in Ground Penetrating Radar Data Enhancement Processing: A Case Study of Embankment Detection in Hunchun City

Fuyu Jiang[1]*, Junkai Yu[1], Likun Gao[2], Jiong Ni[1], Run Han[1], Xiaoyu Xu[1], Haijun Chen[3]

[1]School of Earth Science and Engineering, Hohai University, Nanjing 211100, China

[2]The First Geological Brigade of Jiangsu Geological Bureau, Nanjing 210041, China

[3]Nanjing Hydraulic Research Hydraulic Research Institute, National Energy Administration, Ministry of Transport, Ministry of Water Resources, Nanjing 210029, China

*Corresponding Author: Fuyu Jiang

Abstract:
The quality of ground penetrating radar data is vital for subsequent geological interpretation. Conventional filtering methods often damage the boundary features of geological bodies and affect the accuracy of the interpretation. This paper proposes the use of small sub-domain filtering to enhance ground penetrating radar data. We improve the "Mi" type sub-domain division method and mean square deviation discrimination criterion of traditional small sub-domain filtering. The improved small sub-domain filtering uses the parallelogram division and mean square deviation of the total gradient magnitude as discrimination criterion. Using gprMax to construct geological models of different depths of soft soil and different soil contact interface fluctuations for test, we discuss the effectiveness of traditional and improved small sub-domain filtering in identifying geological body boundaries at different window sizes under the influence of Gaussian noise. Model experiments show that using improved small sub-domain filtering to enhance ground penetrating radar data leads to a higher degree of compression of the phase axis of the geological boundary reflection waves, making them more continuous, clearer, and less deformed. Increasing the filtering window can reflect the boundaries of deep geological structures. In application, the enhanced ground penetrating radar data of the Hunchun City embankment detection show that the improved small sub-domain filtering can preserve the boundary features of geological body boundary, enhance their recognizability, and obtain clearer and more accurate boundary feature information.
Keywords: Ground penetrating radar; Small sub-domain filtering; sub-domain division method; Discrimination criteria; gprMax

Introduction

Ground penetrating radar (GPR) is a non-destructive detection method that uses ultra-high frequency (10^6-10^9 HZ) pulsed electromagnetic waves to determine the distribution of underground media. It has many advantages, such as fast, convenient, and high resolution. The theoretical basis of using this method to detect is that there are obvious dielectric differences within the detection object, such as obvious physical differences between various abnormal bodies (weak interlayers, cavities, water-filled karst caves, etc.) and the surrounding rock. When the electromagnetic wave encounters the boundary of these abnormal bodies during propagation, it will produce a strong reflection phenomenon. Correlation analysis of the received reflection waveform can be used to infer important information such as the spatial location, buried depth, and size of the abnormal body inside the detection object[1–3]. Currently, GPR technology is widely applied in various fields, such as geotechnical engineering surveys, archaeology, engineering quality inspection, and so on[4–6].

Due to the wide frequency band typically used by GPR to record reflected signals, in addition to the reflection signals from abnormal bodies, various noises and other interference signals are inevitably present[7]. Interference signals and effective signals differ in terms of spectrum, energy, and other aspects, which are not the true reflection of the anomalies and need to be suppressed and removed to highlight the effective signals. Therefore, before interpreting the data, the original data must be filtered to minimize the impact of interference signals on the data interpretation, ensuring the accuracy of the interpretation results[8–10]. However, because the boundaries of anomalies often manifest as high-frequency signals, the edges of the anomalies will be blurred during traditional low-pass filtering, thereby reducing the resolution of the anomalies and even distorting the regional characteristics of the anomalies.

To overcome the above drawbacks, a new low-pass filtering method, small sub-domain filtering (SSDF), has been proposed and applied in Bouguer gravity anomaly processing. It has been found that this method can preserve the boundaries of anomalies without significantly damaging them, maintaining the boundary features of the anomalies with a higher resolution[11]. Subsequently, some scholars applied it to the data processing of magnetic anomalies and high-density electrical methods and achieved good results[12,13]. Other researchers have continuously improved the SSDF method to make its filtering output more stable and reasonable. For the sub-domain division method, the window center symmetric division, "Tian" type division, "X" type division and "+" type division, moving type division, ten sub-domain division and other methods are proposed successively. For the discrimination criteria, the average gradient magnitude and the total horizontal derivative mean square deviation are proposed as discrimination criteria[14–20].

Based on previous research, this paper proposes an improved SSDF that adopts a new sub-domain division method and discrimination criteria, and applies it to the enhancement of GPR data. The superiority and practicality of the proposed method are demonstrated through model experiments and the processing of actual data.

2 The principle and improvement of small sub-domain filtering

The SSDF is different from traditional potential field filtering or enhancement methods, such as matched filtering or Wiener filtering, which obtain the output point signal strength by linear filtering based on the signal strength in the neighborhood of the input point based on moving average theory[21,22]. The traditional SSDF method enhances the geological body edge information, first dividing the filter window into sub-domains located on different sides of the window center. Second, it does not calculate the simple weighted average of the whole window but detects anomalous changes in the sub domains during filtering. Then it takes the average sub-domain value using the mean square deviation minimum as the filter output. It is able to achieve a variety of enhancements by locally stretching and squeezing.

This paper improves both the sub-domain division method and the discrimination criteria of the traditional SSDF and proposes an improved SSDF. In terms of the sub-domain division, the traditional SSDF uses a "Mi" type division (Figure 1(a)), whereas the improved SSDF adopts a parallelogram division (Figure 1(b)). Compared with the traditional method, the improved method obtains smaller subdomains and more reasonable results. In terms of the discrimination criteria, the traditional method uses the mean square deviation as the criterion, while the improved method combines the mean square deviation of the original data with the mean square deviation of the total gradient magnitude, commonly used in the recognition of gravity and magnetic anomaly field edges, as the discrimination criterion. This combination reduces the inaccuracy of the results[23,24].

For the improved SSDF method, when the window size is $M \times M$ (where M is an odd number), the specific calculation steps are:

① The mean ΔEz_i and mean square deviation σ_i values are calculated for each sub-domain.

$$\Delta Ez_i = \frac{1}{N}\sum_{j=1}^{N} Ez_i(j) \quad (i = 1, 2, \cdots) \# (1)$$

$$\sigma_i = \sqrt{\sum_{j=1}^{N} \frac{[\Delta Ez_i - Ez_i(j)]^2}{N}} \quad (i = 1, 2, \cdots) \# (2)$$

In equations (1) and (2), ΔEz_i is the mean value of the *i*-th sub-domain, $Ez_i(j)$ is the value of the *j*-th point in the *i*-th sub-domain, σ_i is the mean square deviation value of the *i*-th sub-domain, and N is the number of data points in each sub-domain.

③ Select the top 3 sub-domains with the smallest mean square deviation σ_i as the target region.

④ Calculate the mean value ΔEz_{iASM} and the mean square deviation σ_{iASM} of the total gradient magnitude for the selected 3 sub-domains.

$$\Delta Ez_{iASM} = \frac{1}{N}\sum_{j=1}^{N}\sqrt{\left(\frac{\partial Ez_i(j)}{\partial x}\right)^2 + \left(\frac{\partial Ez_i(j)}{\partial z}\right)^2} \quad (i = 1, 2, 3) \# (3)$$

$$\sigma_{iASM} = \sqrt{\frac{1}{N}\sum_{j=1}^{N}\left(Ez_{i(j)ASM} - \Delta Ez_{iASM}\right)^2} \quad (i = 1, 2, 3) \# (4)$$

In equations (3) and (4), ΔEz_{iASM} is the mean value of the total gradient magnitude of the *i*-th sub-domain, σ_{iASM} is the mean square deviation value of the total gradient magnitude of the *i*-th sub-domain, $Ez_{i(j)ASM}$ is the total gradient magnitude value of the *j*-th point in the *i*-th sub-domain.

⑤ Compare the mean square deviation σ_{iASM} of the total gradient magnitude of the selected 3 sub-domains, and output the mean value of the sub-domain with the smallest mean square deviation of the total gradient magnitude as the center point filtered value of the window.

⑥ Move the filter window to the next point and repeat steps ①~④ until the entire calculation region is covered.

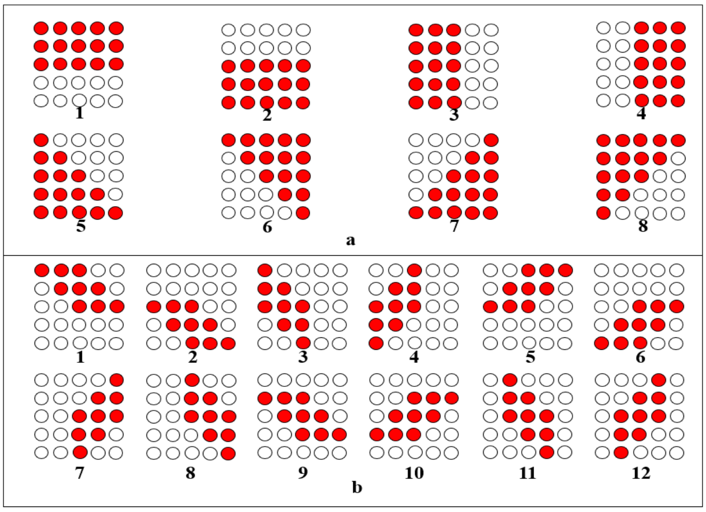

Figure 1 The sub-domain division methods of the SSDF
（a）**Traditional "Mi" type division method;**（b）**Improved parallelogram division method**

3 Model Tests

The previous text theoretically explained the feasibility of using SSDF to enhance GPR data to improve the identification of geological body boundaries. In the following, two models are used as examples to demonstrate the superiority and reliability of the improved SSDF method.

gprMax is an open-source software used to simulate electromagnetic wave propagation. It is based on the Finite Difference Time Domain (FDTD) principle and the Perfectly Matched Layer (PML) boundary absorption condition. Using Yee cells as the spatial discretization units for electromagnetic fields, gprMax converts Maxwell's curl equations into difference equations to solve Maxwell's equations, thereby achieving forward modeling simulations[25–27]. The following tests are simulated using gprMax.

3.1 Model 1

Model 1 is a geological model of different depth soft soil layers shown in Figure 2. The length and height of the model are 8m and 14.5m. The background medium is soil with a relative permittivity of 4, and there is a 0.5m air layer above the soil. The burial depths of the soft soil layers are 4m, 8m, and 12m, with a relative permittivity of 15. In the forward modeling, a Ricker wavelet with a center frequency of 50 MHz is used as the excitation source. The time window is set to 300 ns, and the trace spacing is set to 0.06 m. To study the effects of noise, Gaussian noise with a standard deviation of 5 is added to the forward modeling data.

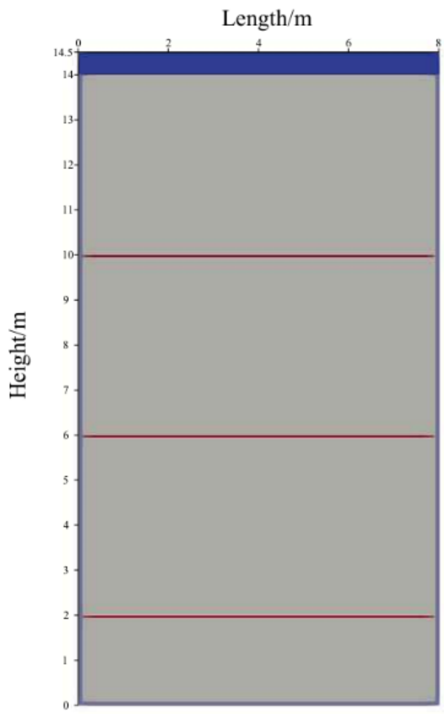

Figure 2 Geological model of different depth soft soil layers

Figure 3 shows the waveform after adding noise. Figure 4 shows the results of the data enhancement processing of Figure 3 using traditional and improved SSDF with different filter window size. Comparing the results of these two types of SSDF, it can be seen that when the filter window size is the same, the improved SSDF obtains a more continuous and clearer reflection wave phase axis of the soft soil layer boundaries (red box area in the figure) after removing the influence of noise. From Figure 5, it can be seen that this phenomenon is due to the improved SSDF has a higher degree of compression of the reflected waves, which increases their amplitude and enhances their energy. Comparing the processing effects of soft soil layers at different depths, it can be seen that in the small filter window, the boundary recognition effect of the soft soil layer at a depth of 4m is better, while the boundary recognition effect of the soft soil layer at depths of 8m and 12m is poor. However, with the increase of the filtering window, the boundary of the soft soil layer with a depth of 8m and 12m is gradually obvious in the figure.

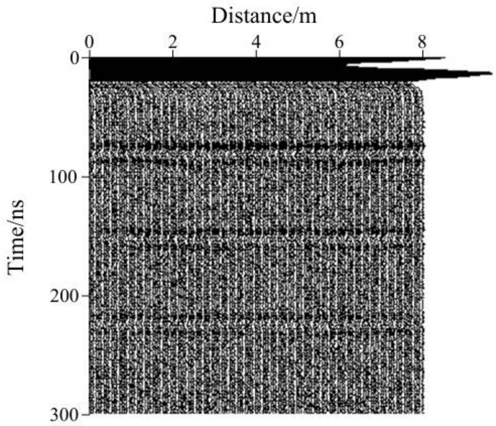

Figure 2 The waveform after adding Gaussian noise with a standard deviation of 5

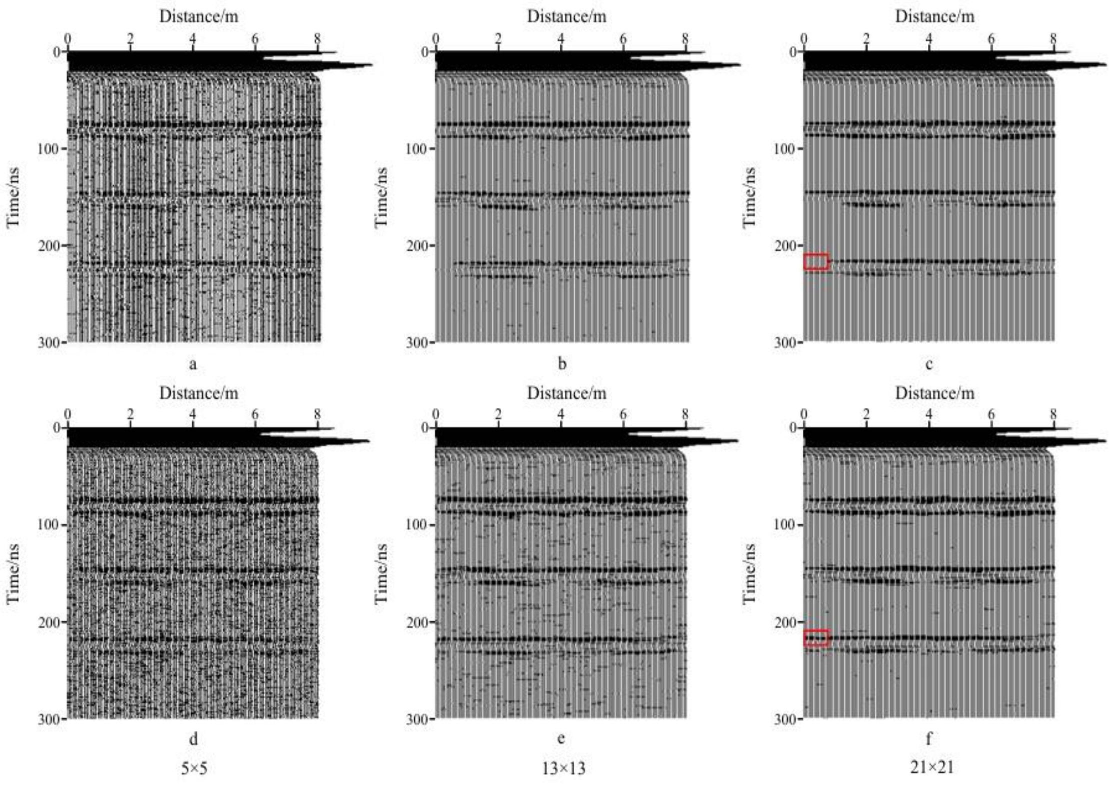

Figure 3 The results of SSDF processing of soft soil layers at different depths
（a）Traditional results of 5×5 window;（b）Traditional results of 13×13 window;
（c）Traditional results of 21×21 window
（d）Improved results of 5×5 window;（e）Improved results of 13×13 window;
（f）Improved results of 21×21 window

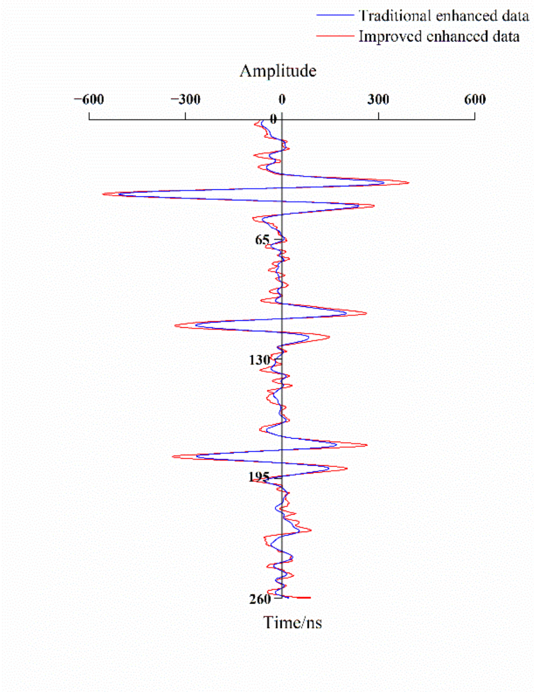

Figure 4 Single-trace SSDF result of soft soil layers at different depths (remove direct wave)

3.2 Model 2

To further study the application effect of the improved SSDF in undulating terrain, a model is designed as shown in Figure 5. The length and height of the model are 6 m and 4.5 m. The upper half of the model is a soil layer with a relative permittivity of 4, and there is an air layer of 0.5 m above it. The lower half is a soil layer with a relative permittivity of 7. In the forward modeling, a Ricker wavelet with a center frequency of 100 MHz is used as the excitation source. The time window is set to 70 ns, and the trace spacing is set to 0.04 m.

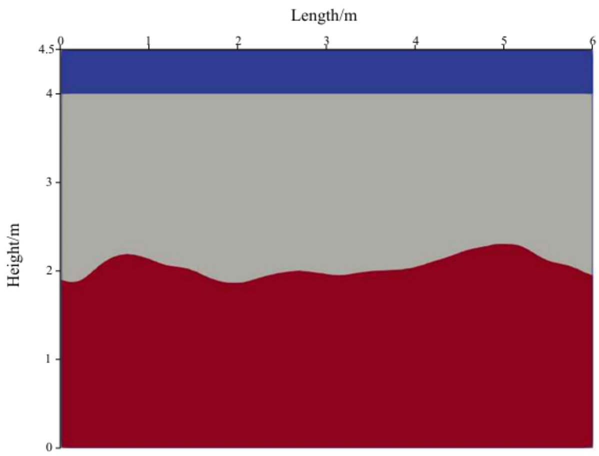

Figure 5 Geological model of different soil contact interface fluctuation

Figure 7 shows the waveform after adding Gaussian noise with a standard deviation of 10. Figure 8 shows the results of the data enhancement processing of Figure 7 using traditional and improved SSDF with different filter window size. Comparing the processing results of these two SSDF, it can be observed that, with the same window size, the improved SSDF is better at preserving the characteristics of the contact boundaries between different soil layers after removing the noise. The reflection wave phase axis is compressed, the shape of the reflection in the undulating areas also more closely matches the original geological model, the deformation degree is lighter, the false anomaly is smaller, and the boundary recognition effect of the geological body is better. As shown in Figure 9, compared to the traditional method, the improved data exhibit a more pronounced variation in the response time of different traces to the contact interface as the undulations of the contact interface change.

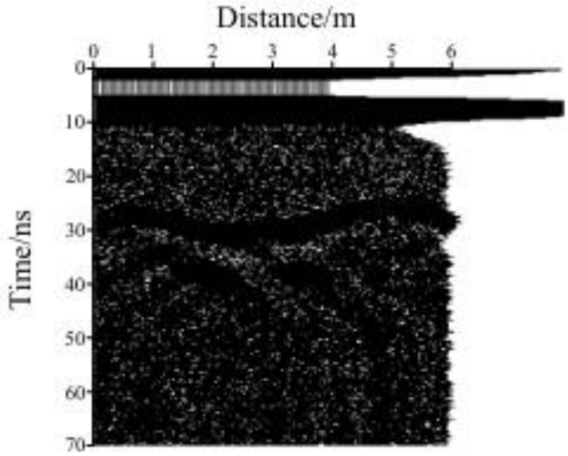

Figure 6 The waveform after adding Gaussian noise with a standard deviation of 10

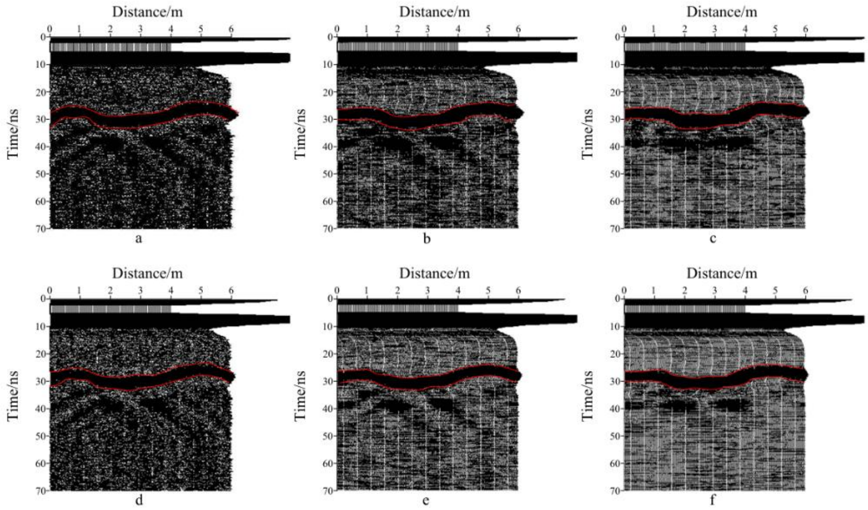

Figure 7 The results of SSDF processing of different soil contact interface fluctuation
（a）Traditional results of 5×5 window;（b）Traditional results of 21×21 window;
（c）Traditional results of 37×37 window
（d）Improved results of 5×5 window;（e）Improved results of 21×21 window;
（f）Improved results of 37×37 window

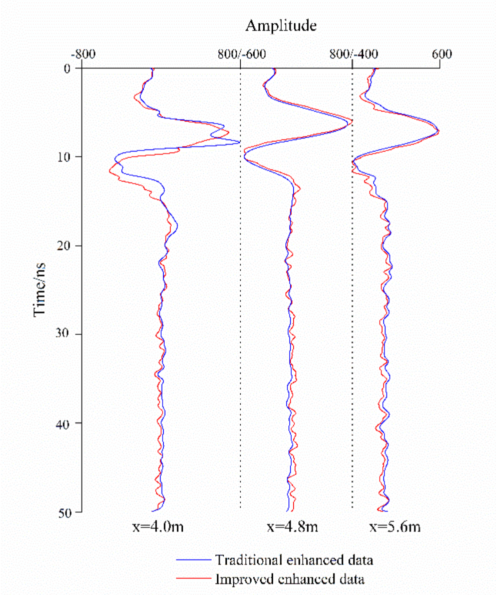

Figure 8 Different trace SSDF result of different soil contact interface fluctuation (remove direct wave)

Figure 10 shows the processing results of the improved SSDF of the different soil contact interface fluctuation when the window size is 77×77. As shown in the figure, as the window size increases, although the noise removal effect improves, the terrain undulations gradually become smoother, which does not align with the shape of the original geological model. Therefore, it is not advisable to choose a large filter window during processing, as it may cause deformation of the geological boundaries, produce false boundary anomalies, and affect the interpretation of results.

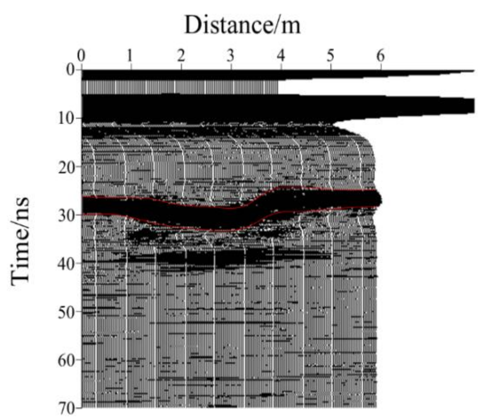

Figure 9 The results of improved SSDF of 77×77 window

Based on the above model tests, it can be concluded that using the improved SSDF for enhancing GPR data, compared to traditional SSDF, better preserves the boundary features of the geological bodies, improves the degree of characterization of these boundaries, and achieves better results in recognizing complex boundary shapes, such as undulating terrain. The identification of deep geological body boundaries can be enhanced by increasing the filter window size, but the window size should not be too large, as this may cause deformation of the boundaries and generate false boundary anomalies.

4 Application

The model tests mentioned above demonstrate the effectiveness of using the improved SSDF to enhance GPR data to improve geological body boundary identification. The following will discuss the practicality of the improved SSDF in GPR data enhancement processing by combining it with embankment detection in Hunchun City.

Hunchun City is located in the eastern part of Jilin Province and southeast of Yanbian Prefecture. It borders the Hassan District of Russia 's Primorsky Krai with the Hunchun Ridge as the boundary. The southwest is adjacent to Rason City in Korea with the Tumen River as the boundary. The north is adjacent to Wangqing County with the Laoye Ridge as the boundary. The northwest corner is connected to the Tumen City, and the northeast is adjacent to Dongning City in Heilongjiang Province. Figure 11 shows the location of the detection area and the layout of the survey line.

Figure 10 The location of the detection area and the layout of the survey line

An SIR-4000 portable GPR is used for detection, and the antenna is equipped with a frequency of 100 MHZ. The time window is set to 200 ns, and the trace spacing is set to 0.01 m. Figure 12 shows a segment of the measured data and its improved SSDF result. As shown in the figure, after the improved SSDF processing, the reflection wave phase axis of different stratum boundaries in the red box are compressed and the boundary features are well-preserved. This enhances recognizability and obtains clearer and more accurate boundary information, thus enabling the creation of a more precise stratigraphic profile, as illustrated in Figure 13.

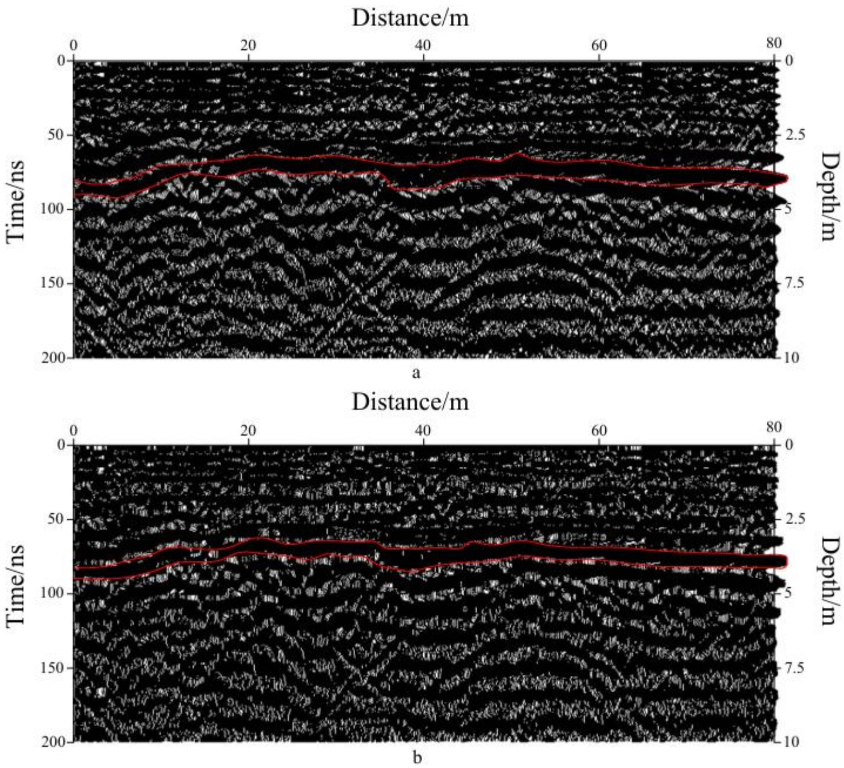

Figure 12 The measured waveform and its improved SSDF result

（a）Measured waveform；（b）Improved results of 21×21 window

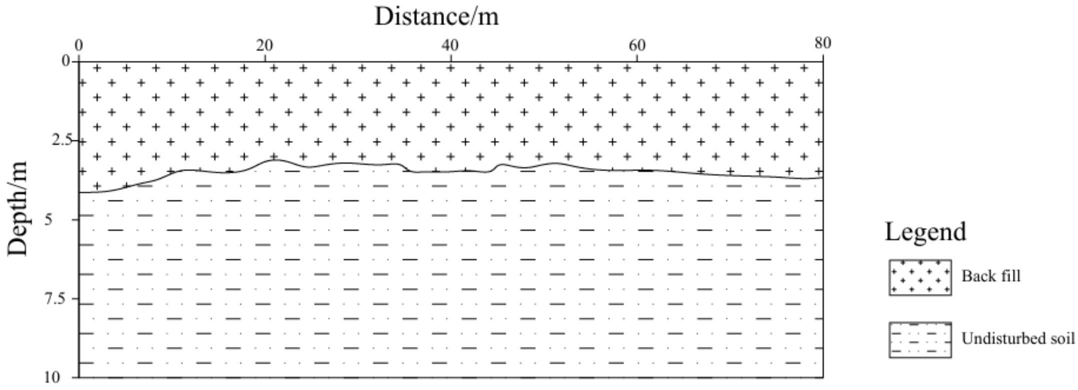

Figure 13 Stratigraphic profile

5 Conclusion

In response to the shortcomings of the traditional SSDF, both sub-domain division and discrimination criteria have been improved. Model experiments have demonstrated that the improved SSDF provides a more refined representation of boundaries than the traditional method. The boundary identification of complex geological bodies is also better and the degree of deformation is lighter. With an increase in the filter window, the boundary of the deep geological body can be better reflected, however, the window should not be too large. In practical applications, the improved SSDF can improve the compression degree of the geological body boundary, preserve the boundary features and improve the visual effect of the geological body boundary in the figure, to obtain clearer and more accurate boundary information.

Funding

This work was supported by the National Key Research and Development Program of China (Grant No. 2021YFC3000103), the National Natural Science Foundation of China (Grant No. 41504081).

Conflicts of Interest

The authors declare no conflict of interest.

References

1. Li, J., Guo, C. C., Wang, F. M., Zhang, J. F. (2007). The summary of the surface ground penetrating radar applied in subsurface investigation. Progress in Geophysics, 22(2): 629-637. DOI: 10.3969/j.issn.1004-2903.2007. 02.043.
2. Ru, R. D., Zhang, J. C., Qi, X. J. (1996). Study on application of ground penetrating radar survey technique. Journal of Engineering Geology, 4(2): 51-56.
3. Yang, L. (2012). The development history and its research status of the technology of ground penetrating radar. Applied Mechanics and Materials, 1975(204-208): 2753-2756. https://doi.org/10.4028/www.scientific.net/AMM.204-208.2753.
4. Xu. X, X., Wu, J., Shen, J. Y., He, Z. C. (2006). Case Study: Application of GPR to Detection of Hidden Dangers to Underwater Hydraulic Structures. Journal of Hydraulic Engineering, 132(1): 12-20. https://doi.org/10.1061 /(ASCE)0733-9429(2006)132:1(12).
5. Cedric, S., Philippe, S., Donatienne, L., Yannick, F., Philippe, C. (2025). Combined GPR and ERT geophysical assessment of a heritage pier. Proceedings of the Institution of Civil Engineers - Maritime Engineering, 1-14. https://doi.org/10.1680/jmaen.24.00018.
6. Wang, Y. P., Jin, H. J., Li, G. Y. (2016). Investigation of the freeze–thaw states of foundation soils in permafrost areas along the China–Russia Crude Oil Pipeline (CRCOP) route using ground-penetrating radar (GPR). Cold Regions Science and Technology, 126: 10-21. https://doi.org/10.1016/j.coldregions.2016.02.013.
7. Su, Z. G., Liao, J. J., Qian, D. H. (2011). The interference signal in GPR survey data and its filtering. Geophysical and Geochemical Exploration, 35(03):427-430.
8. Benedetto, A., Tosti, F., Ciampoli, B. L., Amico, F. (2017). An overview of ground-penetrating radar signal processing techniques for road inspections. Signal Processing, 132: 201-209. https://doi.org/10.1016/j.sigpro.2016.05.016.
9. Zhang, L., Ling, T., Yu, B., Huang, F., Zhang, S. (2021). Intensive interferences processing

for GPR signal based on the wavelet transform and F-K filtering. Journal of Applied Geophysics, 186: 104273. https://doi.org/10.1016/j.jappgeo.2021.104273.

10. Wang, W. T., Du, W., Li, Y. B., Zhuo, J. (2025). Advanced Adaptive Median Filter for Reducing Salt-and-Pepper Noise in GPR Data. IEEE Geoscience and Remote Sensing Letters, 22: 1-5. DOI: 10.1109/LGRS.2025.3532986.
11. Yang, G. Y. (1995). A new technique for potential-field data processing: small subdomain filtering. Oil Geophysical Prospecting, 30(2): 240-244, 291. DOI: 10.13810/j.cnki.issn.1000-7210.1995.02.012.
12. Yan, L. J., Hu, W. B., Yao, C. L. (2006). Filtering enhancement of gravity and magnetic data in the dense ladder-like zone. Progress in Exploration Geophysics, 29(2): 102-103, 4.
13. Yu, J. H., Tao, Y. Z. (2015). Application of small sub-domain filtering to processing of image made by high-density resistivity method. Water Resources and Hydropower Engineering, 46(1): 107-109. DOI: 10.3969/j.issn.1000-0860.2015.01.024.
14. Xiao, F., Wu, Y. G., Meng, L. S. (2010). An improvement on small subdomain filtering in potential field data processing. Oil Geophysical Prospecting, 45(1): 136-139, 164, 175. DOI: 10.13810/j.cnki.issn.1000-7210.2010.0 1.018.
15. Ma, G. Q., Du, X. J., LI, L. L. (2013). An optimized small sub-domain filtering method. Oil Geophysical Prospecting, 48(4): 658-662, 676,506. DOI: 10.13810/j.cnki.issn.1000-7210.2013.04.022.
16. Yan, B., Li, Y., Liu, Z., Ren, S. T., Mukriz, Z. A. I., Chen, Z. M. (2021). Pulse-modulation eddy current imaging and evaluation of subsurface corrosion via the improved small sub-domain filtering method. NDT & E International, 119: 102404. https://doi.org/10.1016/j.ndteint.2021.102404.
17. Tai, Z. H., Wang, Y. H., Zhang, G. H., Li, X. W., Huang, D. Z. (2025). Tensor ratio small subdomain filtering technique for edge detection. Journal of Applied Geophysics, 233:105635-105635. https://doi.org/10.1016/j.jappgeo.2025.105635.
18. Duan, J. X., Xu, Y. (2020). Method and application of edge enhancement of tilt angle based on moving small sub-domain filtering. Progress in Geophysics, 35(6): 2315-2322.
19. Jiang, F. Y., Gao, L. K. (2012). Edge enhancement of gravity anomalies and gravity gradient tensors using an improved small sub-domain filtering method. Applied Geophysics, 9(2): 119-130. DOI:10.6038/pg2020DD0504.
20. Wang, Y. G., Huang, Y. S., Zhang, J. (2020). Gravity interpretation using improved small subdomain filtering of enhanced anomaly. Oil Geophysical Prospecting, 55(1): 206-216, 12-13. DOI:10.13810/j.cnki.issn.1000-7210.2020.01.024.
21. Syberg, F. J. R. (1972). A fourier method for the regional-residual problem of potential fields*. Geophysical Prospecting, 20(1): 47-75. https://doi.org/10.1111/j.1365-2478.1972.tb00619.x.
22. Pawlowski, R. S., Hansen, R. O. (1990). Gravity anomaly separation by Wiener filtering. GEOPHYSICS, 55(5): 539-548. https://doi.org/10.1190/1.1442865.
23. Nabighian, M. N. (1974). Additional comments on the analytic signal of two-dimensional magnetic bodies with polygonal cross-section. Geophysics, 39(1): 85-92. https://doi.org/10.1190/1.1440416.
24. Wang, W. Y. (2012). Spatial variation law of the extreme value position of analytical signal amplitude for potential field data. Chinese Journal of Geophysics, 55(4): 1288-1299. DOI: 10.6038/j.issn.0001-5733.2012.04.024.
25. Warren, C., Giannopoulos, A., Giannakis, I. (2016). gprMax: Open source software to simulate electromagnetic wave propagation for Ground Penetrating Radar. Computer Physics Communications, 209: 163-170. https://doi.org/10.1016/j.cpc.2016.08.020.
26. Kane, Y. (1966). Numerical solution of initial boundary value problems involving maxwell's equations in isotropic media. IEEE Transactions on Antennas and Propagation, 14(3):302-307. DOI: 10.1109/TAP.1966.1138693.
27. Giannopoulos, A. (2005). Modelling ground penetrating radar by GprMax. Construction and Building Materials, 19(10): 755-762. https://doi.org/10.1016/j.conbuildmat.2005.06.007.